Book Chapter

Evolution of Char Structure During In-Situ Biomass Tar Reforming: Importance of the Coupling Effect Among the Physical-Chemical Structure of Char-Based Catalysts

Dongdong Feng, Yu Zhang, Yijun Zhao and Shaozeng Sun

School of Energy Science and Engineering, Harbin Institute of Technology, China

***Corresponding Author:** Dongdong Feng, School of Energy Science and Engineering, Harbin Institute of Technology, Harbin 150001, China

Published **March 20, 2020**

This Book Chapter is a republication of an article published by Dongdong Feng, et al. at Catalysts in August 2019. (Zhang, Y.; Feng, D.; Zhao, Y.; Dong, H.; Chang, G.; Quan, C.; Sun, S.; Qin, Y. Evolution of Char Structure During In-Situ Biomass Tar Reforming: Importance of the Coupling Effect Among the Physical-Chemical Structure of Char-Based Catalysts. Catalysts 2019, 9, 711.)

How to cite this book chapter: Dongdong Feng, Yu Zhang, Yijun Zhao and Shaozeng Sun. Evolution of Char Structure During In-Situ Biomass Tar Reforming: Importance of the Coupling Effect Among the Physical-Chemical Structure of Char-Based Catalysts. In: Ayuk Eugene Lakem, editor. Prime Archives in Chemistry. Hyderabad, India: Vide Leaf. 2020.

Author Contributions: Y.Z., D.F., Y.Z., and S.S. conceived and designed the experiments; D.F. and Y.Z. performed the experiments; Y.Z., D.F., Q.C., and G.C. analyzed the data; Y.Z., H.D., and Y.Q. contributed reagents/materials/analysis tools; Y.Z. and D.F. wrote the paper.

Funding: This work was supported by the National Natural Science Foundation of China (51906052), the National Postdoctoral Program for Innovative Talents of China (BX20180086), China Postdoctoral Science Foundation Funded Project (2018M641826), Heilongjiang Provincial Postdoctoral Science Foundation, and Fundamental Research Funds for the Central Universities (HIT. NSRIF. 2020052).

Conflicts of Interest: The authors declare no conflict of interest.

Abstract

In order to illustrate the importance of a coupling effect in the physical-chemical structure of char-based catalysts on in-situ biomass tar reforming, three typical char-based catalysts (graphite, Zhundong coal char, and sawdust biochar) were studied in the fixed-bed/fluidized-bed reactor. The physical-chemical properties of carbon-based catalysts associated with their catalytic abilities were characterized by inductively coupled plasma-atomic emission spectroscopy (ICP-AES), Raman, X-ray photoelectron spectroscopy (XPS), scanning electron microscope–energy dispersive spectrometer (SEM-EDS) and N_2 adsorption. The relationship between the specific reactivity and tar reforming ability of carbon-based catalysts was discussed through a micro fluidized bed reaction analyzer (MFBRA–MR). The results indicate that the char-based catalyst has certain removal ability for in-situ biomass tar of corn straw in an inert atmosphere, which is as follows: sawdust biochar > Zhundong (ZD) coal char > graphite. During the in-situ tar reforming, the alkali and alkaline earth metal species (AAEMs) act as adsorption/reaction sites, affecting the evolution of the aromatic

ring structure and oxygen-containing functional groups of the char-based catalyst, and also its pore structure. AAEM species on the surface of char-based catalysts are the active sites for tar reforming, which promotes the increase of active intermediates (C-O bond and C-O-AAEMs), and enhances the interactions between char-based catalysts and biomass tar. The abundant AAEMs may lead to the conversion of O=C–O and C=O to C–O. For tar reforming, the internal pore structure of char-based catalysts is little changed, mainly with the carbon deposit forming on the surface pore structure. The carbon deposit from the reformation of straw tar on the char surface has better reactivity than the inherent carbon structure of ZD coal char and sawdust biochar. There is a positive relationship between the MFBRA–MR specific reactivity and tar catalytic reforming ability of char-based catalysts (decided by the coupling effect in their physical-chemical structure), which can be used to determine the catalytic ability of char-based catalysts on tar reforming directly.

Keywords

Biomass Tar; Reforming; Char; Physicochemical Structure; Coupling Effect

Nomenclature

AAEMs- Alkali and Alkaline Earth Metallic Species; ZD coal-Zhundong Coal; ICP-AES- Intrepid Inductively Coupled Plasma Atomic Emission Spectrometer; XPS- X-ray Photoelectron Spectroscopy; SEM-EDS- Scanning Electron Microscopy-Energy Dispersive Spectrometer; BDDT- Brunauer, Deming, Deming, and Teller; MFBRA–MR- Micro Fluidized Bed Reaction Analyzer–MS Reactor

Introduction

During biomass gasification, tar is undesirable because of various problems associated with condensation, formation of tar aerosols, and polymerization to form more complex structures [1-4]. Tar can be defined as a complex mixture of condensable hydrocarbons, which includes single ring to 5-ring aromatic

compounds, along with other oxygen-containing hydrocarbons and complex polycyclic aromatic hydrocarbons (PAH) [5]. Tar concentrations in the syngas from the gasification of low rank fuel vary from 5 to 75 g/(Nm^3) [6-9], which is much higher than the maximal allowance for the utilization of syngas in gas turbines and engines, ranging from 10 to 50 mg/(Nm^3) [10]. Among the approaches for tar destruction, catalytic reforming is gaining widespread acceptance due to its overall high efficiency [11]. Char-based catalyst is one of the products from pyrolysis/gasification of coal or biomass that has a strong catalytic ability on biomass tar reforming [3,12].

The main catalytic mechanisms of tar conversion in the char-based materials include deposition, dehydrogenation (carbon deposited on the surface of char), and carbon consumption [4,13,14]. The physical-chemical structures of char-based catalysts are all important factors affecting catalytic ability of tar reforming [15,16]. For pore structure, it has been proven that a char-based catalyst has high affinity and strong adsorption selectivity for hydrocarbons [17]. The mesopores of char-based catalysts are thought to be effective in converting heavy hydrocarbons into light components, while limiting the formation of carbon deposits. The catalytic performance of biochar (char-based catalyst) with its high toluene removal rate was due to its large surface area/pore volume and better pore size distribution [18]. The highly porous structures of char-based catalysts not only greatly improve the dispersion of inherent metal catalytic elements, but also promote the transfer of reactant molecules (e.g., toluene, 0.68 nm molecular size) to the inner surface of catalysts [19]. The alkali and alkaline earth metal species (AAEMs) in biomass or coal char play an important role in tar catalytic reforming, showing that a char-based catalyst could promote the conversion of alkyl mono-aromatic hydrocarbons and inhibit the formation of polycyclic aromatic hydrocarbons (PAHs) [20,21]. The connection between carbon matrix and AAEM species would protect the structure of small aromatic rings from volatilization, and the dispersion of AAEM species would be deteriorated with the enrichment of large aromatic rings in char-based catalysts [22]. More importantly, the char chemical structures are significant in affecting the

inherent metal-carbon interactions, thus affecting their catalytic performances [3,23]. Increasing the number of surface oxygen-containing functional groups could promote the adsorption/reforming of biomass tar compounds [24,25]. The content of oxygen-containing functional groups was mainly in the form of acidic groups, which reduced the pH_{pzc} of the char-based catalyst and enhanced its catalytic activity [26]. The chemical structure, including carbon skeleton structure and O-containing functional groups, would not only show catalytic activity itself, but also largely govern the roles and fates of AAEM species and thus its catalytic performance [27]. Therefore, it is of paramount importance to investigate the evolution of char structure during in-situ biomass tar reforming, especially for the importance of the coupling effect within its physical-chemical structure.

Therefore, the objective of this work was to examine the total tar catalytic reforming abilities and dynamic evolution of related physical-chemical properties of char-based catalysts (especially for their coupling effect) during the in-situ biomass tar reforming. Different carbonaceous materials (i.e., biomass, coal, and graphite) were used in this study so as to formulate different char-based catalysts with various physical-chemical structures, in order to evaluate their coupling effect on tar reforming.

Results and Discussion

Tar Yield, Tar Removal Rate and Weight Change of Char-Based Catalysts

The results of in-situ biomass tar reforming over three char-based catalysts are shown in Figure 1a,b, with a clear picture in Supplementary Materials (1). The main components of tar can be seen in Supplementary Materials (2), which is not the focus of research. The tar yield over sawdust biochar is 2.00%, which is the lowest one, while its removal rate of tar is 46.9%. The tar removal rate of Zhundong (ZD) coal char and graphite is 39.2% and 19.6%, respectively. It can be concluded that the char-based catalyst has a certain removal ability for in-situ biomass tar of corn straw in an inert atmosphere, which is as follows: Sawdust biochar > ZD coal char > graphite.

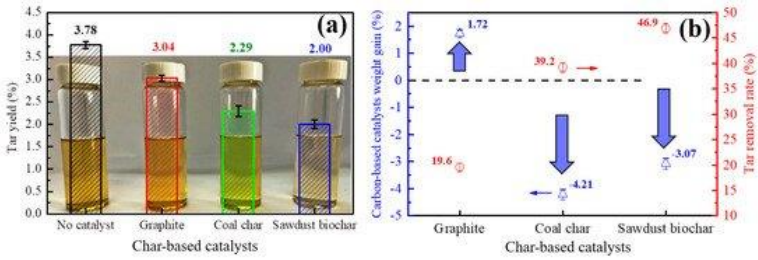

Figure 1: In-situ biomass tar reforming results over char-based catalysts: (**a**) Tar yields, and (**b**) weight gain and tar reforming rate for the char-based catalysts.

As shown in Figure 1b, it can be found that graphite shows slight weight gain after the tar reforming reaction, while ZD coal char and sawdust biochar show significant weight losses, which is due to H/O/OH radicals in the volatile matter from corn straw pyrolysis reacting with the active structures of coal char and biochar [28]. These free radicals participate in the tar reforming on the char surface, and O/OH radicals can activate the activation/gasification of active carbon atoms in the char sample. At the same time, the H radical would have the ability to inhibit the consumption of char [29]. ZD coal char and sawdust biochar are more active in contact with in-situ volatiles from corn straw because of their abundant AAEM species and active physical-chemical structures; thus, they have larger tar reforming rates. The adsorption and reorganization of tar over graphite are limited, due to its simple structures and few active sites for tar reforming. The inhibition of H radicals on the gasification of graphite becomes obvious, and the char's consumption is limited [30]. Therefore, the weight gain of graphite appears after the in-situ biomass tar reforming.

AAEMs Species in Char-Based Catalysts

The total content of AAEM species in ZD coal char is higher than that in sawdust biochar, with mass fractions of 1.71% and 1.39%, respectively, as show in Figure 2a,b. The Ca element accounts for the highest proportion in char-based catalysts, which reaches 1.18% in coal char and 0.89% in biochar, while the species with the second highest content are K (in biochar)

and Na (in coal char). In addition to the inherent properties of the raw material's own elemental distribution, the precipitation characteristics of the AAEM species during its preparation also play an important role. Due to the unstable single bond between monovalent K/Na and carbon matrix, they would have a large amount of volatilization during preparation, while that of the divalent Ca might be relatively stable [31,32]. It shows that K and Na elements account for 0.38% in ZD coal char, while elements of sawdust biochar account for 0.43%. In addition, it can be found that the AAEMs content in char-based catalysts and their tar removal abilities are not consistent, for the reason that not all AAEM species are with "catalytic activity" for biomass tar reforming [33]. A large number of AAEM species in the char-based catalysts are encapsulated in the carbon matrix. AAEM species exposed to the gas–solid interface of char-based catalysts could be able to show their effective catalytic ability for tar reforming.

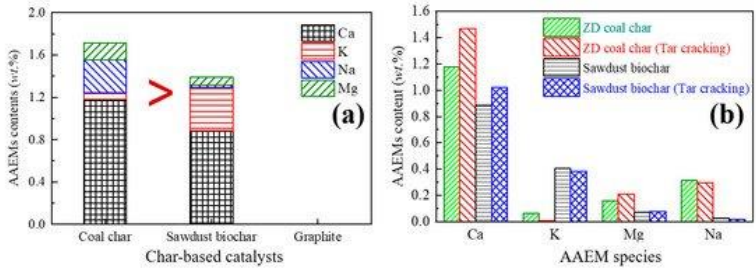

Figure 2: Alkali and alkaline earth metal species (AAEMs) contents in char-based catalysts: (**a**) Raw and (**b**) changes before/after tar reforming.

As shown in Figure 2b, it is found that the contents of AAEM species in the coal char and biochar after tar reforming show a similar trend. Ca and Mg increase slightly, while Na and K decrease. A large number of H/O/OH radicals in the gas phase can easily destroy the chemical bonds between K/Na and carbon matrix, resulting in their volatilization [31], while leaving the active sites and defects of the carbon structure to promote the adsorption of tar molecules. Ca and Mg elements are stable in connection with the carbon matrix, which are not easy to volatilize. Meanwhile, Ca and Mg could directly participate in the tar adsorption and reorganization. During the in-situ tar

reforming, the AAEM species act as adsorption/reaction sites, and the reaction process will have a significant effect on the evolution of the aromatic ring structure and oxygen-containing functional groups of the char-based catalyst, and the effect on its pore structure would also be prominent to a certain extent. New bonds are formed between Ca/Mg and active tar intermediates; thus, tar can be removed due to the surface carbon gasification on the gas–solid interface. The raw corn straw materials contain high Ca and Mg, so the increase of Ca and Mg in char-based catalysts after a reaction can be due to the attachment of Ca and Mg elements in in-situ volatility from corn straw pyrolysis. Thus, it can be proposed that K/Na elements could exhibit catalytic activity at the gas–solid interface of char, due to their easier migration and transformation during the homogeneous/heterogeneous reforming of biomass tar. In contrast, the catalytic activity of Ca is relatively weak.

Chemical Structures of Char-Based Catalysts

For the Raman analysis, it was believed that the total peak area was directly related to the number of oxygen-containing structures and the degree of aromatization [31], while the former may be more significant. As shown in Figure 3a, there are only obvious D and G peaks in graphite, while the total peak area of graphite after tar reforming increases significantly. This may be explained by the abundant oxygen-containing functional group structure in the carbon deposit structure after tar reforming, and/or how the oxidation of O/OH radicals in volatile matter onto graphite leads to the formation of C–O, C=O chemical bonds, which enhances the Raman scattering of graphite. The lack of oxygen-containing functional groups and high degree of aromatization in graphite are not conducive to tar reforming [21]. The total peak area of ZD coal char and sawdust biochar is much larger, indicating more oxygen-containing functional groups. The total peak area of the two char-based catalysts decreases after tar reforming reaction, indicating that the surface groups are consumed. Sawdust biochar needs to consume more during tar reforming, indicating that sawdust biochar is more easily deactivated than ZD coal char. During tar reforming in an inert atmosphere, the formation of carbon deposits would

continuously block the active sites on the surface of char-based catalysts and inhibit the catalytic abilities of AAEM species and oxygen-containing functional groups. The Raman spectra of coal char and biochar catalysts are fitted by a peak-fitting method, which can be obtained in our previous investigation [34]. As shown in Figure 3b, the I_D/I_G is used to describe the crystal structure and graphite-like functional group structure of char, while $I_D/I_{(Gr+Vl+Vr)}$ and I_D/I_{Gr} represent the abundance of large aromatic ring structures in char-based catalysts [31]. It can be found that the I_D/I_G ratio of sawdust biochar before reaction is higher than that of ZD coal char, indicating that the carbon structural defects of sawdust biochar are more than those of ZD coal char, which has a positive effect on tar reforming activity. The ratios of $I_D/I_{(Gr+Vl+Vr)}$ and I_D/I_{Gr} of ZD coal char are higher than those of sawdust biochar, showing that the proportion of large aromatic rings in the structure of ZD coal char was higher, which was not conducive to the total tar removal results. Thus, it can highlight the importance of the coupling effect among the physical-chemical structures of char-based catalysts. After tar reforming, the ID/IG ratio of sawdust biochar increases, while that of ZD coal char decreases. Tar molecules undergo depolymerization and dealkylation at high temperature in gas phase. Active H/O/OH radicals in the volatiles from corn straw pyrolysis could react with tar molecules to form activated tar fragments, which gradually connect to lattice defects of char and then undergo further reforming reaction [35], accompanying the catalytic effects of AAEM species in this process. The reaction increases the aromaticity of char and decreases the number of lattice defects in sawdust biochar. The final result is that I_G increases while I_D decreases. For ZD coal char, the tar compounds bound to the char can be reformed from the char surface by bond breaking, which may be detached as a part of the char structure, resulting in the increase of lattice defects with the increase of I_D/I_G ratio. For the changes of $I_D/I_{(Gr+Vl+Vr)}$ and I_D/I_{Gr} before and after tar reforming, it was found that the ratio of large aromatic rings to small aromatic rings increased. Similar to the results of I_D/I_G, H/O/OH volatile radicals preferentially consume small aromatic rings and form large aromatic rings, resulting in the increases of $I_D/I_{(Gr+Vl+Vr)}$ and I_D/I_{Gr} ratios. The consumption of small aromatic rings is more serious during tar

reforming, resulting in the better tar catalytic reforming activity. Thus, during the tar reforming, the changes of the aromatic ring structures and the surface functional groups of char-based catalysts are synergistic.

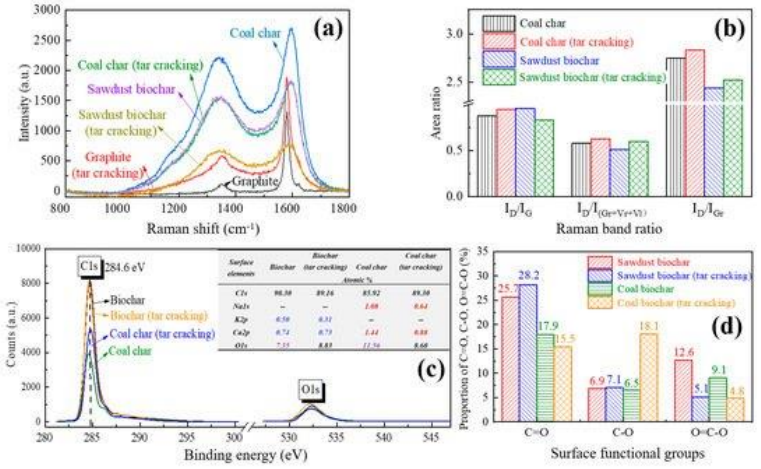

Figure 3: Chemical characteristics of char-based catalysts on in-situ biomass tar reforming: (**a**) Raman spectra; (**b**) Raman band ratio; (**c**) C1s and O1s peaks in XPS spectra; and (**d**) Proportion of C=O, C–O, O=C–O functional groups.

The distribution of active AAEM species and oxygen-containing functional groups on the surface (1–10 nm) of char-based catalysts can be seen in Figure 3c,d. The proportion of O=C–O functional groups of the coal char and biochar decreases significantly after tar reforming, while the proportion of C–O functional groups increases. This indicates that the consumption of oxygen functional groups is mainly carboxyl or lipid groups during reaction. The proportion of C=O and C–O functional groups increased slightly, due to the consumption of O=C–O. The conversion of C=O and O=C–O functional groups to C–O functional groups also occurs in ZD coal char. K and Ca on the surface of char-based catalysts are the active sites for tar reforming, which promotes the increase of active intermediates (C–O bond and C–O–K/Ca) [36], and enhances the interactions between char-based catalysts and biomass tar. Therefore, the abundant AAEMs may lead to the conversion of O=C–O and C=O to C–O in ZD coal char. As shown in Figure 3d, Na^{1s}, K^{2p},

and Ca^{2p} represent the structure and electronic arrangement of Na, K, and Ca elements on the char surface, respectively. The surface oxygen content of ZD coal char is higher than that of sawdust biochar before reaction. The proportion of O-containing functional groups in ZD coal char was higher than that in sawdust biochar (e.g., 32.94% and 25.29%, respectively). The proportion of AAEM species on the surface of ZD coal char is still higher than that of sawdust biochar (e.g., 1.24% and 2.52%, respectively), which indicates that the surface active sites of ZD coal char are more. After tar reforming, the content of Na, Ca, and O in ZD coal char change in varying degrees, while the content of K in sawdust biochar decreases significantly and the content of O increases. It indicates that more breaks and/or reconnections of chemical bonds occur on the surface of ZD coal char during tar reforming. The sawdust biochar might remove more tar by adsorption, so the consumption of various active sites is relatively small.

Physical Structures of Char-Based Catalysts

The specific surface area, pore volume, and pore size ratios of three char-based catalysts can be seen in Table 1. Higher porosity and surface area enhance the contacting chances between char and tar [37,38], while enabling more active sites to attach to the char surface. After tar reforming, the surface area and pore volume of three char-based catalysts decreased significantly, due to the formation of carbon deposit, which is mainly formed on the surface active sites (such as AAEMs and surface active groups/structures). From the pore size distribution, it is found that there are only a few micropores in graphite, but no macropore in graphite. The micropore is dominant in sawdust biochar and ZD coal char. After tar reforming, the micropore number of the three char-based catalysts decreased in varying degrees, while that of graphite decreased slightly, confirming that the adsorption of tar by graphite was mostly carried out between the lamellae. The decrease of micropores in sawdust biochar was especially obvious, and the content of meso/macropores increased significantly after tar reforming. The H/O/OH radicals in volatile matter make contact with the carbon matrix, which leads to the expansion of a large number of

micropores, and the collapse of pore walls and the connection between pores. For another reason, the carbon deposit blocked the pores and formed a larger pore structure in the process of aggregation on/around the microporous surface, resulting in a sharp decrease in the proportion of micropores, but an increase of meso/macropores. The abundant meso/macroporous structure, which makes up the main active sites [37], makes sawdust biochar have a larger "active surface area", which is conducive to its tar reforming ability.

Table 1: N_2 adsorption parameters of three char-based catalysts.

Conditions	BET Surface Area (m^2/g)	Pore Volume (cm^3/g)	Micropore Area <2 nm (m^2/g)	Large Hole Area >2 nm (m^2/g)	$S_{Mic.}/S_{Ext.}$
Graphite	0.29	0.0029	3.18	- -	- -
Coal char	13.73	0.0107	10.42	3.31	3.15
Sawdust biochar	188.86	0.1069	139.68	49.18	2.84
Graphite (tar reforming)	0.04	0.0018	3.15	- -	- -
Coal char (tar reforming)	1.77	0.0040	1.28	0.48	2.67
Sawdust biochar (tar reforming)	89.66	0.0845	11.89	77.77	0.15

The adsorption isotherm curves between the nascent char and tar-reformed char can reflect the dynamic properties of surface pore structure, based on the BDDT theory [39]. The N_2 adsorption/desorption isotherm curves of sawdust biochar and ZD coal char are shown in Figure 4a,b. Compared with typical curves, sawdust biochar and ZD coal char before reaction belong to IV curves (e.g., mesopore solid obtained by Suuberg E M. et al. [40]). Multilayer adsorption occurs on the surface of the adsorbent, and the pore size distribution is mostly microporous and microporous [41,42]. It is found that the two char-based catalysts do not form a complete loop structure, indicating that the char particles with such desorption curves had "ink bottle" pores or a complex network structure [39]. After tar reforming, the N_2 adsorption content of ZD coal char and sawdust biochar decreases significantly. The sawdust biochar is due to the massive blockage of micropores and the formation of a macroporous structure by carbon deposit, and the overall

adsorption capacity decreases. It shows that the pore structure of sawdust biochar can play a durable role in tar reforming. The adsorption/desorption curves of the two char-based catalysts after reaction basically coincide, indicating that the internal pore structure of char is little changed and the quantity is limited, most of which consists of disconnected holes with an opening at one end.

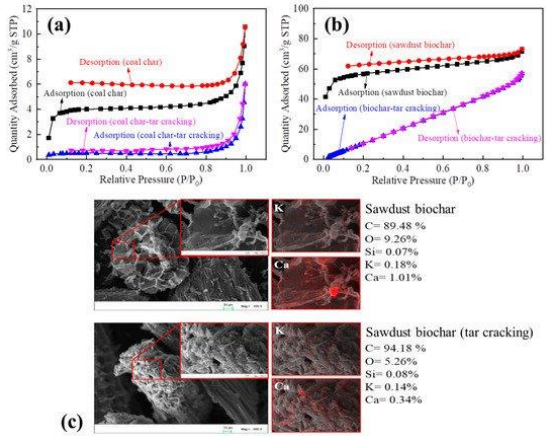

Figure 4: Physical characteristics of char-based catalysts on in-situ biomass tar reforming: Isothermal nitrogen adsorption/desorption curves of (**a**) coal char and (**b**) sawdust biochar; (**c**) SEM-EDS results of sawdust biochar.

The SEM-EDS results of three char-based catalysts can be seen in Figure 4c and Supplementary Materials (3-a, 3-b, 3-c). As shown in Supplementary Materials (3-a), the raw graphite is a strict lamellar structure with orderly arrangement, without obvious pore structure, and slightly interstitial between the lamellae. After tar reforming, the graphite surface was covered by viscous carbon deposits, and the surface showed a continuous hilly structure. The adsorption process plays an absolute role between graphite and biomass tar. The formation and distribution of AAEMs (e.g., Ca), together with tar in the pore structure of graphite, reflect the important role of AAEM species in the homogeneous transformation of tar [35]. In addition, during heterogeneous reforming, AAEMs are precipitated together with volatile matter from corn straw, which will adhere/bond to the surface of the char-based catalyst [43] and

participate in the heterogeneous reforming reaction of biomass tar. After tar reforming, the graphite surface contains a small amount of O, which is consistent with the result of Raman analysis. In Supplementary Materials (3-b), unreacted ZD coal char has a relatively regular morphology, which is a partially fractured honeycomb structure, with more pore structures than graphite. After tar reforming, it was found that the pore structures of ZD coal char were blocked by carbon deposit, and more carbon deposits were accumulated in the pore-rich areas. From the distribution of surface elements, it is found that the surface of ZD coal char is rich in O, that is, it has more oxygen-containing functional group structure, while more AAEM species such as Ca, Na, and Mg, are evenly distributed on the char surface. After tar reforming, the AAEMs content decreases due to their volatilization and the formation of carbon deposit. Figure 4c and Supplementary Materials (3-c) show that the surface of sawdust biochar before reaction consists of mainly strip-like fibrous structures. The surface pore structure is mostly macroporous and irregular. During tar reforming, the carbon deposition is observed to encapsulate the fiber structure and adhere to the macroporous structure, while the overall structure is still disorderly and loose. On its distribution of surface elements, it has an abundance of O, Ca, and K content. Compared with ZD coal char, sawdust biochar has a more dense distribution of catalytic elements, especially for enrichment of Ca at the fiber fracture. The content of Ca, K, and O in sawdust biochar decreases after tar reforming, which indicates that the porous structure may promote the catalytic reaction of AAEM species and active chemical structures on the char surface, thus promoting the adsorption and reforming of biomass tar.

Reactivities of Char-Based Catalysts

The absolute conversion rate, relative conversion rate, and carbon reaction rate during the combustion of char-based catalysts are obtained, as shown in Figure 5a,b. It can be found that although the relative carbon conversion rate of graphite is faster, the carbon consumption after the reaction is only 0.725% and 1.579%, showing that graphite barely reacts during combustion at 600 °C. The absolute carbon conversion rate of

sawdust biochar is much higher than that of ZD coal char and graphite, indicating that sawdust biochar has higher combustion activity. The combustion activity of sawdust biochar changed slightly before and after tar reforming, and the combustion reaction rate of sawdust biochar increased slightly after tar reforming. The change of ZD coal char is obvious, and the amount of carbon consumed after tar reforming increases significantly, which indicates that the carbon deposited after tar reforming has higher combustion activity than that of ZD coal char. After tar reforming, the peak values of the combustion reaction rate curves of the two char-based catalysts shift to the right, indicating that tar reforming reduces the intensity of the initial combustion of char-based catalysts and prolongs the combustion time. It indicates that the carbon deposit formed by the reformation of straw tar on the catalyst surface has better reactivity than the inherent carbon structure of ZD coal char and sawdust biochar. The results show that there is a positive correlation between the combustion activity and tar reforming activity of different kinds of char-based catalysts. The results are attributed to the coupling effect in the physical-chemical structure (e.g., pore structure, AAEMs, surface active groups, and aromatic structures) of char-based catalysts, which are not only the key factors affecting tar reforming ability in an inert atmosphere, but are also the important factors affecting the combustion activity.

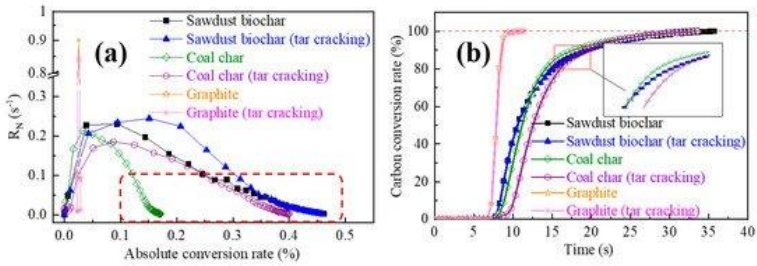

Figure 5: Reactivity analysis of char-based catalysts on in-situ biomass tar reforming from a micro fluidized bed reaction analyzer (MFBRA–MR): (**a**) Reaction rate versus absolute carbon conversion rate and (**b**) carbon conversion rate with time.

Experimental

Preparation of Char-Based Catalysts

Manchurian walnut sawdust, obtained from Harbin, Heilongjiang Province, China, was used in the experiments. The sawdust samples were dried overnight at 105 °C, pulverized, and sieved to obtain a fraction with particle sizes between 0.15 and 0.25 mm. The proximate and ultimate analyses for the sawdust samples are listed in Table 1.

Three kinds of char-based catalysts, namely, graphite, Zhundong (ZD) coal char, and sawdust biochar, were selected for the in-situ tar catalytic reforming, and were prepared in a standard muffle furnace, which can be seen in our previous paper [35]. Raw materials were dried at 105 °C for 12 h, grinded, and screened to 150–250 μm. Corn straw (e.g., 150–250 μm) with AAEM species in corn straw (0.60 wt. % Na_2O, 29.41 wt. % K_2O, 18.38 wt. % MgO, and 14.34 wt. % CaO in ash), obtained from the farmland in Harbin, China, was used for pyrolysis to supply the in-situ biomass tar. The proximate and ultimate analysis of three kinds of raw materials is shown in Table 2.

Table 2: Proximate and ultimate analysis of the origin sample. (Note: Diff. = by difference, ad. = air dry basis, daf. = dry ash-free basis).

Sample Name	Proximate Analysis (ad., %)				Ultimate Analysis (daf., %)				
	Moisture	Volatile	Ash	Fixed Carbon	C	H	N	S	$O_{diff.}$
ZD coal	9.63	40.30	5.50	44.57	61.40	4.41	0.89	0.48	17.69
Sawdust	9.49	77.13	0.96	12.42	43.72	5.31	0.12	0.01	40.39
Corn stalk	6.17	71.20	6.52	16.11	40.39	5.14	1.12	0.16	39.91

In-Situ Biomass Tar Reforming Over Char-Based Catalysts

In-situ biomass tar reforming experiments were carried out in a fixed-bed/fluidized-bed experimental system in Ar atmosphere at 800 °C, as shown in Figure 6. Biomass tar was from the corn straw pyrolysis in the bottom fluidized-bed stage and then passed through the intermediate frit into the upper fixed-bed stage (in

which the char-based catalysts were pre-loaded), where the in-situ catalytic reforming of biomass tar over char-based catalysts was carried out. For the outlet, the reacted tar was trapped in two gas bottles, which were connected in series and filled with a solvent mixture of HPLC-grade chloroform and methanol (4:1, v/v), which were put into an ice brine bath (≤0 °C). Calculation of tar yield and tar conversion rate can be seen in our previous research papers [35].

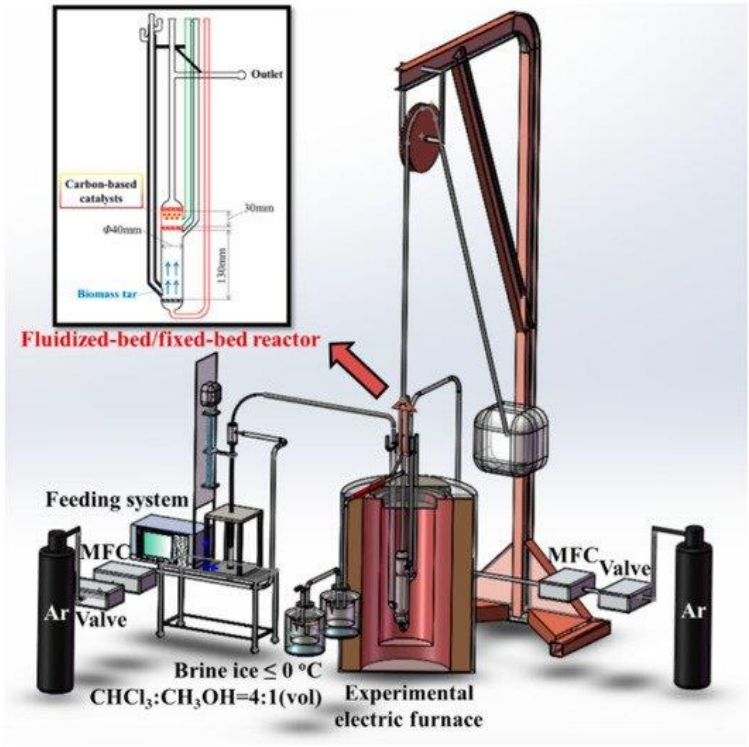

Figure 6: Experimental system of fixed-bed/fluidized-bed reactor.

Analysis of Physical-Chemical Structures of Char-Based Catalysts

The specific surface area, pore size, and pore volume distribution of char-based catalysts were measured by N_2 adsorption (ASAP 2020M, Micromeritics Instrument Crop, USA).

The char-based catalyst was digested by an Ethos-1 microwave digestion instrument of MILESTONE company in Italy. Then, 65% HNO_3, 30% H_2O_2, and 40% HF were selected as high-grade pure reagents. The amount of char-based catalyst was 0.10 g during digestion. The liquids collected were analyzed for AAEMs concentration using IRIS Intrepid Inductively Coupled Plasma Atomic Emission Spectrometer (ICP-AES).
The carbon structure of the char-based catalyst was tested by a Raman Spectrometer of Renishau Company, United Kingdom. The device was equipped with a 1040 × 256 charge coupled device camera for focusing laser beams on samples and was equipped with an in-Via Confocal microscope, Renishaw CCD detector, and excitation laser with a wavelength of 633 nm. The spectra of about 800–1800 cm^{-1} were recorded at five different locations for each char sample, and then the average value was obtained.

X-ray photoelectron spectroscopy (XPS) uses X-rays to excite valence or inner electrons of atoms or molecules. The instrument is equipped with a 1486.6 Ev monochrome Al Kα X-ray spectrometer. The narrow-spectrum scanning transmission energy of the sample used is 50 eV and the scanning step is 0.1 eV. The data are calibrated by linear shifts, where the maximum peak of C1s binding energy corresponds to 284.6 eV. The functional groups and elemental properties of the surface are analyzed using the number of escaped electrons from the char surface at depths of 1–10 nm.

EVO18 scanning electron microscopy (SEM) and an X-MAX20 energy dispersive spectrometer (EDS) of Carl Zeiss Co. from Germany were used to scan the surface characteristics of char-based catalysts with a magnification of up to 2000 times and to determine the elemental composition on the surface of samples.

Reactivity of char-based catalysts was studied by the micro fluidized bed reaction analyzer (MFBRA–MR) [44]. Combustion tests were carried out at 600 °C with a mixed gas atmosphere of 21%O_2/79%Ar. The measured response value can be converted into gas concentration by the reliable positive proportional

relationship between the signal response value and concentration, for subsequent analysis of the carbon conversion rate.

Conclusions

- The char-based catalyst has a certain removal ability for in-situ biomass tar of corn straw in an inert atmosphere, which is as follows: sawdust biochar > ZD coal char > graphite.
- During the in-situ tar reforming, the AAEM species act as adsorption/reaction sites, affecting the evolution of the aromatic ring structure and oxygen-containing functional groups of the char-based catalyst, and also its pore structure. AAEM species on the surface of char-based catalysts are the active sites for tar reforming, which promotes the increase of active intermediates (C–O bond and C–O–AAEMs), and enhances the interactions between char-based catalysts and biomass tar. The abundant AAEMs may lead to the conversion of O=C–O and C=O to C–O.
- For tar reforming, the internal pore structure of the char-based catalyst is little changed, mainly with the carbon deposit forming on the surface pore structure. The carbon deposit from the reformation of straw tar on the char surface has better reactivity than the inherent carbon structure of ZD coal char and sawdust biochar.
- There is a positive relationship between the MFBRA–MR specific reactivity and tar catalytic reforming ability of char-based catalysts, which can be used to determine the catalytic ability of char-based catalysts on tar reforming directly.

References

1. Devi L, Ptasinski KJ, Janssen FJ. A review of the primary measures for tar elimination in biomass gasification processes. Biomass Bioenergy. 2003; 24: 125–140.
2. Sipra AT, Gao N, Sarwar H. Municipal solid waste (MSW) pyrolysis for bio-fuel production: A review of effects of

MSW components and catalysts. Fuel Process. Technol. 2018; 175: 131–147.
3. Zhang S, Chen Z, Zhang H, Wang Y, Xu X, et al. The catalytic reforming of tar from pyrolysis and gasification of brown coal: Effects of parental carbon materials on the performance of char catalysts. Fuel Process. Technol. 2018; 174: 142–148.
4. Wang Y, Hu X, Mourant D, Song Y, Zhang L, et al. Evolution of aromatic structures during the reforming of bio-oil: Importance of the interactions among bio-oil components. Fuel 2013; 111: 805–812.
5. Li C, Suzuki K. Tar property, analysis, reforming mechanism and model for biomass gasification—An overview. Renew. Sustain. Energy Rev. 2009; 13: 594–604.
6. Coll R, Salvado J, Farriol X, Montane D. Steam reforming model compounds of biomass gasification tars: Conversion at different operating conditions and tendency towards coke formation. Fuel Process. Technol. 2001; 74: 19–31.
7. Kurkela E, Ståhlberg P. Air gasification of peat, wood and brown coal in a pressurized fluidized-bed reactor. I. Carbon conversion, gas yields and tar formation. Fuel Process. Technol. 1992; 31: 1–21.
8. Zhang R, Wang Y, Brown RC. Steam reforming of tar compounds over Ni/olivine catalysts doped with CeO_2. Energy Convers. Manag. 2007; 48: 68–77.
9. Kinoshita C, Wang Y, Zhou J. Tar formation under different biomass gasification conditions. J. Anal. Appl. Pyrolysis. 1994; 29: 169–181.
10. Bridgwater A. The technical and economic feasibility of biomass gasification for power generation. Fuel. 1995; 74: 631–653.
11. Liu Q, Xiong Z, Syed-Hassan SSA, Deng Z, Zhao X, et al. Effect of the pre-reforming by Fe/bio-char catalyst on a two-stage catalytic steam reforming of bio-oil. Fuel. 2019; 239: 282–289.
12. Zhang S, Asadullah M, Dong L, Tay HL, Li CZ. An advanced biomass gasification technology with integrated catalytic hot gas cleaning. Part II: Tar reforming using char as a catalyst or as a catalyst support. Fuel. 2013; 112: 646–653.

13. Hosokai S, Norinaga K, Kimura T, Nakano M, Li CZ, et al. Reforming of Volatiles from the Biomass Pyrolysis over Charcoal in a Sequence of Coke Deposition and Steam Gasification of Coke. Energy Fuels. 2011; 25: 5387–5393.
14. Shao S, Zhang H, Xiao R, Li X, Cai Y. Evolution of coke in the catalytic conversion of biomass-derivates by combined in-situ DRIFTS and ex-situ approach: Effect of functional structure. Fuel Process. Technol. 2018; 178: 88–97.
15. Li CZ. Importance of volatile–char interactions during the pyrolysis and gasification of low-rank fuels—A review. Fuel. 2013; 112: 609–623.
16. Hu C, Zhang H, Xiao R. Effects of nascent char on ex-situ catalytic fast pyrolysis of wheat straw. Energy Convers. Manag. 2018; 177: 765–772.
17. Xu CC, Hamilton S, Ghosh M. Hydro-treatment of Athabasca vacuum tower bottoms in supercritical toluene with microporous activated carbons and metal–carbon composite. Fuel. 2009; 88: 2097–2105.
18. Bhandari PN, Kumar A, Bellmer DD, Huhnke RL. Synthesis and evaluation of biochar-derived catalysts for removal of toluene (model tar) from biomass-generated producer gas. Renew. Energy. 2014; 66: 346–353.
19. Feng D, Zhao Y, Zhang Y, Sun S, Meng S, et al. Effects of K and Ca on reforming of model tar compounds with pyrolysis biochar under H_2O or CO_2. Chem. Eng. J. 2016; 306: 422–432.
20. Zhang Y, Kajitani S, Ashizawa M, Oki Y. Tar destruction and coke formation during rapid pyrolysis and gasification of biomass in a drop-tube furnace. Fuel. 2010; 89: 302–309.
21. Wang FJ, Zhang S, Chen ZD, Liu C, Wang YG. Tar reforming using char as catalyst during pyrolysis and gasification of Shengli brown coal. J. Anal. Appl. Pyrolysis. 2014; 105: 269–275.
22. Li X, Hayashi JI, Li CZ. Volatilisation and catalytic effects of alkali and alkaline earth metallic species during the pyrolysis and gasification of Victorian brown coal. Part VII. Raman spectroscopic study on the changes in char structure during the catalytic gasification in air. Fuel. 2006; 85: 1509–1517.

23. El-Rub ZA, Bramer EA, Brem G. Experimental comparison of biomass chars with other catalysts for tar reduction. Fuel. 2008; 87: 2243–2252.
24. Song Y, Wang Y, Hu X, Xiang J, Hu S, et al. Effects of volatile–char interactions on in-situ destruction of nascent tar during the pyrolysis and gasification of biomass. Part II. Roles of steam. Fuel. 2015; 143: 555–562.
25. Song Y, Wang Y, Hu X, Hu S, Xiang J, et al. Effects of volatile–char interactions on in situ destruction of nascent tar during the pyrolysis and gasification of biomass. Part I. Roles of nascent char. Fuel. 2014; 122: 60–66.
26. Ducousso M, Weiss-Hortala E, Nzihou A, Castaldi MJ. Reactivity enhancement of gasification biochars for catalytic applications. Fuel. 2015; 159: 491–499.
27. Feng D, Zhao Y, Zhang Y, Gao J, Sun S. Changes of biochar physiochemical structures during tar H_2O and CO_2 heterogeneous reforming with biochar. Fuel Process. Technol. 2017; 165: 72–79.
28. Shen Y. Chars as carbonaceous adsorbents/catalysts for tar elimination during biomass pyrolysis or gasification. Renew. Sustain. Energy Rev. 2015; 43: 281–295.
29. Fushimi C, Wada T, Tsutsumi A. Inhibition of steam gasification of biomass char by hydrogen and tar. Biomass Bioenergy. 2011; 35: 179–185.
30. Tay HL, Kajitani S, Zhang S, Li CZ. Inhibiting and other effects of hydrogen during gasification: Further insights from FT-Raman spectroscopy. Fuel. 2014; 116: 1–6.
31. Feng D, Zhao Y, Zhang Y, Xu H, Zhang L, et al. Catalytic mechanism of ion-exchanging alkali and alkaline earth metallic species on biochar reactivity during CO_2/H_2O gasification. Fuel. 2018; 212: 523–532.
32. Jiang L, Liu C, Hu S, Wang Y, Xu K, et al. Catalytic behaviors of alkali metal salt involved in homogeneous volatile and heterogeneous char reforming in steam gasification of cellulose. Energy Convers. Manag. 2018; 158: 147–155.
33. Zhou W, Bai B, Chen G, Ma L, Jing D, et al. Study on catalytic properties of potassium carbonate during the process of sawdust pyrolysis. Int. J. Hydrog. Energy. 2018; 43: 13829–13841.

34. Zhao Y, Feng D, Zhang Y, Huang Y, Sun S. Effect of pyrolysis temperature on char structure and chemical speciation of alkali and alkaline earth metallic species in biochar. Fuel Process. Technol. 2016; 141: 54–60.
35. Feng, D., Zhao, Y., Zhang, Y., Sun, S. Effects of H_2O and CO_2 on the homogeneous conversion and heterogeneous reforming of biomass tar over biochar. Int. J. Hydrog. Energy 2017, 42, 13070–13084.
36. Feng D, Zhao Y, Zhang Y, Zhang Z, Sun S. Roles and fates of K and Ca species on biochar structure during in-situ tar H2O reforming over nascent biochar. Int. J. Hydrog. Energy. 2017; 42: 21686–21696.
37. Mun TY, Kim JW, Kim JS. Air gasification of dried sewage sludge in a two-stage gasifier: Part 1. The effects and reusability of additives on the removal of tar and hydrogen production. Int. J. Hydrog. Energy. 2013; 38: 5226–5234.
38. Klinghoffer NB, Castaldi MJ, Nzihou A. Catalyst Properties and Catalytic Performance of Char from Biomass Gasification. Ind. Eng. Chem. Res. 2012; 51: 13113–13122.
39. Sing KSW. Reporting physisorption data for gas/solid systems with special reference to the determination of surface area and porosity (Provisional). Pure Appl. Chem. 1982; 54: 2201–2218.
40. Suuberg EM, Deevi SC, Yun Y. Elastic behaviour of coals studied by mercury porosimetry. Fuel. 1995; 74: 1522–1530.
41. Zhao Y, Feng D, Li B, Sun S, Zhang S. Combustion characteristics of char from pyrolysis of Zhundong sub-bituminous coal under O_2/steam atmosphere: Effects of mineral matter. Int. J. Greenh. Gas Control. 2019; 80: 54–60.
42. Zhao Y, Feng D, Li B, Wang P, Tan H, et al. Effects of flue gases ($CO/CO_2/SO_2/H_2O/O_2$) on NO-Char interaction at high temperatures. Energy. 2019; 174: 519–525.
43. Du C, Liu L, Qiu P. Importance of volatile AAEM species to char reactivity during volatile–char interactions. RSC Adv. 2017; 7: 10397–10406.
44. Liu P, Zhao Y, Guo Y, Feng D, Wu J, et al. Effects of volatile-char interactions on char during pyrolysis of rice husk at mild temperatures. Bioresour. Technol. 2016; 219: 702–709.

Supplementary Materials

Supplement materials can be accessed online at: https://videleaf.com/wp-content/uploads/2020/03/PACHEM-19-14_Supplementary-Materials.pdf

Supplement Material (1): Vials picture of tar samples with char-based catalysts, Supplement Material (2): Main components of tar by GC-MS without char-based catalysts, Supplement material (3): SEM EDS results of char based catalysts.